International Journal of Pharmaceutics 423 (2012) 471–479

Contents lists available at SciVerse ScienceDirect

International Journal of Pharmaceutics

journal homepage: www.elsevier.com/locate/ijpharm

Preparation, characterization and *in vivo* assessment of the bioavailability of glycyrrhizic acid microparticles by supercritical anti-solvent process

Xiaoyu Sui[a,1], Wei Wei[b,1], Lei Yang[a,*], Yuangang Zu[a,**], Chunjian Zhao[a], Lin Zhang[a], Fengjian Yang[a], Zhonghua Zhang[a]

[a] *Key Laboratory of Forest Plant Ecology, Ministry of Education, Northeast Forestry University, Harbin 150040, China*
[b] *College of Life Science, Nanjing University, Nanjing 210093, China*

ARTICLE INFO

Article history:
Received 27 July 2011
Received in revised form 26 October 2011
Accepted 5 December 2011
Available online 13 December 2011

Keywords:
Glycyrrhizic acid
Microparticles
Supercritical anti-solvent
Oral bioavailability

ABSTRACT

In this study, glycyrrhizic acid (GA) microparticles were successfully prepared using a supercritical anti-solvent (SAS) process. Carbon dioxide and ethanol were used as the anti-solvent and solvent, respectively. The influences of several process parameters on the mean particle size (MPS), particle size distribution (PSD) and total yield were investigated. Processed particle sizes gradually decreased as temperature and solution flow rate increased. In addition, processed particle sizes increased from 119 to 205 nm as GA concentration increased. However, CO_2 flow rate did not significantly affect particle size. The optimized process conditions were applied, those included temperature (65 °C), pressure (250 bar), CO_2 and drug solution flow rate (15 and 8 mL min^{-1}), drug concentration in ethanol (20 mg mL^{-1}). Microparticles with a span of PSD ranging from 95 and 174 nm, MPS of 128 nm were obtained, and total yield was 63.5%. The X-ray diffraction patterns of glycyrrhizic acid microparticles show apparent amorphous nature. Fourier transform infrared (FT-IR) spectroscopy results show that no chemical structural changes occurred. The *in vitro* dissolution tests showed that the GA microparticles exhibited great enhancement of dissolution performance when compared to GA original drug. Furthermore, the *in vivo* studies revealed that the microparticles provided improved pharmacokinetic parameter after oral administration to rats as compared with original drug.

1. Introduction

Liquorice, the root of the leguminous *Glycyrrhiza* plant species, has been used since ancient Egyptian, Greek, and Roman times in the West and since the Former Han era (the 2nd–3rd century B.C.) in ancient China in the East., and is one of the most frequently employed botanicals in foods and traditional medicines (Shibata, 2000). Glycyrrhizic acid (GA) is a terpenoid compound (Fig. 1) and is the main active ingredient of liquorice. It is 30–50 times sweeter than sugar and is used widely as a sweetening additive in the food industry. GA has various pharmacological effects such as anti-HIV, anti-tumor, anti-inflammatory and hepatoprotective (Cherng et al., 2004; Finney and Somers, 1958; Lin et al., 1999; Nishino et al., 1984). However, GA have poor water solubility, in this case, its dissolution in biological liquids is also practically poor. Therefore, the oral bioavailability of GA is slightly low. In order to solve this problem, various GA preparations have been researched in recent years. These include GA liposome (Yuan et al., 2005), GA-chitosan nanoparticles delivery system (Lin et al., 2008), cyclodextrin inclusion complexes (Cui et al., 2008).

The application of microparticles is a common and popular method to enhance the dissolution rate of poorly water-soluble drugs. Microparticles have the smaller particle size compared to raw drug particles which can lead to an increase in interfacial surface area and consequently improvement of drug solubility in water. Consequently, microparticles can improve bioavailability and oral efficacy, allowing for smaller dosages and more rapid and direct usage of the poorly water-soluble drugs. Many techniques have been developed for microparticles preparation, including co-melting of a drug–carrier mixture, dissolution of the drug and carrier in a mutual solvent with subsequent solvent evaporation (solvent evaporation method), spray drying, ultra fine grinding (Li et al., 2008; Ma et al., 2009; Rizi et al., 2010). However, drawbacks or limitations associated with these methods are as follows: relatively large particle size and particle size distribution, difficulties

* Corresponding author at: Box 332, Northeast Forestry University, Hexing Road 26, Harbin, Heilongjiang Province, China. Tel.: +86 451 82191314; fax: +86 451 82102082.
** Corresponding author at: Box 332, Northeast Forestry University, Hexing Road 26, Harbin, Heilongjiang Province, China. Tel.: +86 451 82191517; fax: +86 451 82102082.
E-mail addresses: leiyangnefu@gmail.com (L. Yang), zygorl@126.com (Y. Zu).
[1] These authors contributed equally to this work.

0378-5173/$ – see front matter © 2011 Elsevier B.V. All rights reserved.
doi:10.1016/j.ijpharm.2011.12.007

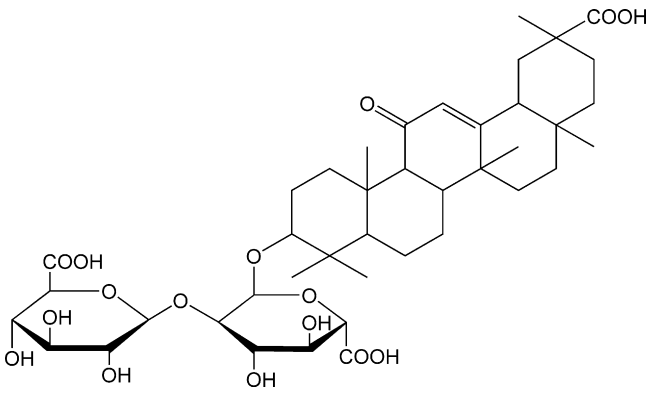

Fig. 1. Chemical structure of glycyrrhizic acid.

in complete recovery of organic solvents, residual organic solvent represent a potential toxicological risks.

Supercritical anti-solvent (SAS) process is an available technology to prepared drug microparticles, without the need for grinding procedure. In this process, the drug is firstly dissolved in the solvent and then the drug solution is quickly sprayed into supercritical fluids (the anti-solvent). Precipitation occurs immediately by a rapid recrystallization of the drug. In general, SAS process can control particle size of production within the nanometer range, moreover the solvent can be fully recovered, is an environmentally friendly technology. In SAS process, operating parameters have a great influence on particle size and PSD, such as temperature, pressure, drug concentration, etc. (Yang et al., 2011; Zhao et al., 2011).

Therefore, the objective of this study is to confirm the feasibility of SAS process to prepare GA microparticles, and investigate the change of dissolution rate and bioavailability between GA microparticles and raw GA particles. This study also attempts to determine the influence of different process parameters on the MPS, PSD and total yield. Thus we can obtain optimized process parameters for GA microparticles preparation. Moreover, characterization of the prepared GA microparticles was examined by scanning electron microscopy (SEM), Fourier transform infrared spectroscopy, thermogravimetry analysis (TGA) and X-ray diffraction (XRD). In vitro dissolution tests in deionized water at 37 °C were carried out. Furthermore, we investigated the effect of microparticles on the pharmacokinetic parameters of GA after a single oral dose of GA in healthy rats.

2. Materials and methods

2.1. Materials

GA (98% pure, MPS = 28 μm) was obtained from Xi'an Sino-herb Biotechnology Co., Ltd. (Shanxi, China). Reference compound of GA (≥98%) was purchased from J&K Chemical Ltd (Beijing, China). High purity CO_2 (99.99% pure) was purchased from Liming Gas Company of Harbin (Heilongjiang, China). Ethanol (analytically pure) was purchased from Beijing Chemical Reagents Company (Beijing, China). Deionized water was prepared by a Milli-Q water-purification system (Millipore, Bedford, MA, USA) and was used in all experiments.

2.2. Preparation of GA microparticles

A schematic diagram of the SAS apparatus that was used in this study is shown in Fig. 2. The apparatus consists of three main parts: feeding, precipitation chamber and gas–liquid separation chamber. Firstly, GA solution was prepared in ethanol. The CO_2 is dried in a silica gel dryer (3), and then is cooled in a gas cooler (4) before be compressed by a high pressure piston pump (5), flow rate of liquid CO_2 was measured by a flowmeter (6). After pre-heated through a heat exchanger (7), supercritical carbon dioxide enters the 1000 cm^3 precipitation chamber (9), the pressure and temperature in the precipitation chamber are measured by a pressure gauge manometer with an accuracy of ±1.6 bar (YB-150A, Tianli Controller Manufacturing Co., China) and a thermometer with an accuracy of ±0.8 °C (WSS-511, Hongde Control Technology Co., China), respectively. The pressure of the precipitation chamber can be adjusted using a back pressure regulator (12). Once the precipitation vessel reached steady state (above critical temperature and pressure), the GA solution (total volume, 120 mL) of is pumped (20), heated (21) and fed into the precipitation chamber through a capillary nozzle (inner diameter = 150 μm; length = 10 cm). This nozzle is located in a distinct inlet port from the SC-CO_2, but also at the top of the precipitation chamber. A stainless steel frit vessel of 200 nm was placed at the bottom of the chamber to collect the GA microparticles and to let the SC-CO_2/ethanol solvent mixture pass through the chamber. The pressure in the precipitation chamber is measured by a pressure gauge manometer. The outflow is regulated by a valve (13) located between the precipitation chamber and the gas–liquid separation chamber (16). This valve is heated with an electric cable in order to prevent the freezing of carbon dioxide due to the rapid depressurization.

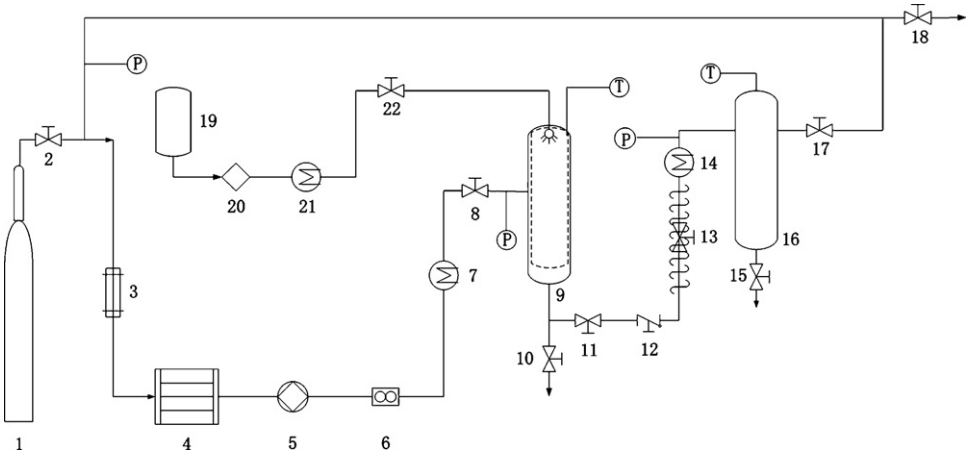

Fig. 2. Schematic diagram of the experimental apparatus for the SAS process. 1, CO_2 source; 3, silica gel dryer; 4, gas cooler; 5, high pressure piston pump; 6, flowmeter; 7, 14 and 21, heat exchanger; 2, 8, 10, 11, 13,15, 17, 18 and 22, valves; 9, precipitation chamber; 12, back pressure regulator; 16, gas–liquid separation chamber; 19, liquid solution supply; 20, solution metering pump.

The mixture suffers a decompression to separate the CO_2 from the ethanol solvent in the gas–liquid separation chamber. Usually the temperature of the vessel is around 15 °C and pressure ≤5 MPa. The pressure in the separation chamber is measured by a pressure gauge manometer.

At the end of the precipitation process, the vessel is washed with the antisolvent to remove the residual solvent. The liquid solution flow was then stopped and a pure constant carbon dioxide flow was maintained in order to completely change the volume of the precipitator and thus to remove the residual solvent. After this washing step which lasted approximately 90 min, depressurization lasted 30 min at the experimental temperature.

2.3. Particle characterization

2.3.1. Particle size analysis

Number average particle diameters and number average particle size distribution of the prepared microparticles were measured by dynamic light scattering (DLS) using particle size analyzer laser (BI-90Plus, Brookhaven Instruments Co., USA). The sample was dispersed in deionized water (no surfactant was used in water) and sonicated for 5 min at 100 W (KQ-100VDE, Kunshan Ultrasonic Instruments Co., China). Three replicate measurements were carried out at 25 °C with a temperature controlled system.

2.3.2. Scanning electron microscopy

The samples were fixed to an SEM stub with a carbon conductive and sputter-coated with gold using sputter-coater (KYKY SBC-12, Beijing, China). The surface morphology of particle was then observed by SEM using a Quanta 200, FEI scanning electron microscope (FEI Company, USA).

2.3.3. X-ray diffraction

The patterns of pure materials and microparticles were obtained using the X-ray diffractometer (Philips, Xpert-Pro, The Netherlands) with Ni-filtered Cu-Kα radiation. Measurement was performed at a voltage of 40 kV and 30 mA. Samples were scanned from 3° to 45°, and the scanned rate was 1° per minute.

2.3.4. Fourier transform infrared spectroscopy

The FT-IR spectra of samples were obtained on an IRAffinity-1 FT-IR spectrophotometer (Shimadzu Co., Japan). Every sample and potassium bromide were mixed by an agate mortar and compressed into a thin disc. The scanning range was 400–4000 cm^{-1} and the resolution was 4 cm^{-1}.

2.3.5. Differential scanning calorimetry and thermal gravimetric analysis

Differential scanning calorimetry (DSC) measurements were performed on a Setaram DSC 131 scanning calorimeter (Setaram Co., France). Samples of 15 mg were placed in aluminum pans and sealed in the sample pan press. The probes were heated from 25 to 300 °C at a rate of 10 °C min^{-1} under nitrogen atmosphere.

Thermogravimetry analysis of samples was carried out with a PerkinElmer Pyris 1 TGA instrument (Perkin-Elmer Co., USA). The experiments were performed with a heating rate of 10 °C min^{-1} using nitrogen flow (50 mL min^{-1}) and samples were weighed (approximately 5 mg) in open aluminum pans and the percentage weight loss of the samples was monitored from 50 to 450 °C.

2.3.6. Dissolution study

The accurate weight of raw material and microparticle of GA were respectively added into 100 mL phosphate buffer (pH = 6,8). Bath temperature and paddle speed were set at 37 ± 1 °C and 100 r min^{-1}. At selected time intervals, 2 mL aliquots were withdrawn using a syringe adapted to a 0.22 μm-filter and replaced by fresh media. Filtered samples were appropriately diluted with methanol and assayed for drug concentration by HPLC. Chromatographic analyses were performed on a Waters HPLC system consisting of a pump (Model 1525), an auto-sampler (Model 717 plus), UV detector (2487 Dual λ absorbance detector). The C_{18} column (Diamonsil, 5 μm, 4.6 mm × 250 mm, Dikma technologies) was used at 25 °C. The mobile phase consisted of 80% methanol and 20% water delivered at 1.0 mL min^{-1}. The injection volume was 10 μL. The signal was monitored at 246 nm. The linear regression equations for reference compound of GA is $Y_{GA} = 7.488 \times 10^6 X + 12{,}8020$ ($r^2 = 0.9996$) A good linearity was found for GA in the range of 0.005–1.5 mg mL^{-1}, respectively. Dissolution experiments were carried out in triplicate. The dissolution profiles were plotted as the cumulative dissolution concentration versus incubation time.

2.4. Bioavailability study of GA microparticles in rats

The animals used for *in vivo* experiments were Wistar male rats (200–250 g). The animals were kept under standard laboratory conditions, temperature at 25 ± 2 °C and relative humidity (55 ± 5%). The rats (total 6 rats) were deprived of food overnight and deprived of water for 5 h before the experiment. Drug suspensions were given orally using oral feeding sonde under ether anaesthesia. The dose given to each rat was calculated based on the weight of the rat, 250 mg of GA per kilogram body weight. The pharmacokinetic analysis was conducted using Practical Pharmacokinetic Program-Version 97 (3P97, published by Chinese Pharmacological Association, Beijing, China).

3. Results and discussion

3.1. Effect of operating conditions on the MPS and yield of GA microparticles

In the SAS process, the size and morphology of the particles can be manipulated by adjusting the parameters, such as flow rate, pressure and temperature of CO_2 or drug concentration. Furthermore, the microparticle yield is also correlated with operating parameters. For this reason, in this study, we investigated the effect of various experimental conditions on microparticle size and yield. We first consider the MPS (as small as possible) of the GA microparticles and then we consider the yield (as high as possible) when optimizing the SAS process. The experimental conditions and results are summarized in Table 1.

3.1.1. Effect of temperature and pressure

The effect of temperature was investigated by varying precipitation temperature at 35, 45, 55 and 65 °C while maintaining all other variables constant: operation pressure of 200 bar, drug concentration of 20 mg mL^{-1}, the flow rates of CO_2 and drug solution were 10 mL min^{-1} and 6 mL min^{-1}. The effect of the temperature on the MPS and yield of microparticles was shown in Fig. 3a. In the figure, the top and bottom of each gray bar represent the upper and lower limit of PSD, respectively. The white circle represents the MPS. An increase in temperature from 35 to 65 °C causes a reduction in the MPS from 293 nm to 156 nm. This behavior can be explained on the basis of the numerical modeling of mass transfer proposed by Werling and Debenedetti (1999). At miscible conditions, a higher mass-transfer rate is produced with increasing temperature at high pressure. Therefore, a higher degree of supersaturation is achieved, which can lead to a higher nucleation rate. Meanwhile, higher diffusivity was obtained with increasing temperature, and thus results in a smaller particle size. Such an effect has also already been observed in the micronization of nicotinic acid and was illustrated that this behavior is directly related to the solubility improvement of the

Table 1
Experimental conditions and results of the supercritical anti-solvent micronization of GA.

No.	Temperature (°C)	Pressure (bar)	CO_2 flow rate (mL min^{-1})	Solution flow rate (mL min^{-1})	Concentration (mg mL^{-1})	Molar ratio of ethanol to CO_2	MPS and average span (nm)	Yield (%)
1	35	200	10	6	20	0.59	293, 133	54.2
2	45	200	10	6	20	0.59	238, 126	57.2
3	55	200	10	6	20	0.59	197, 96	65.5
4	65	200	10	6	20	0.59	156, 78	69.3
5	65	150	10	6	20	0.59	283, 115	72.6
6	65	200	10	6	20	0.59	166, 86	66.4
7	65	250	10	6	20	0.59	139, 68	62.2
8	65	300	10	6	20	0.59	209, 85	46.8
9	65	250	10	6	20	0.59	143, 79	64.8
10	65	250	15	6	20	0.39	150, 91	61.5
11	65	250	20	6	20	0.29	132, 73	51.4
12	65	250	25	6	20	0.23	130, 77	40.2
13	65	250	15	4	20	0.26	189, 106	65.9
14	65	250	15	6	20	0.39	148, 99	63.8
15	65	250	15	8	20	0.52	133, 67	60.2
16	65	250	15	10	20	0.65	124, 55	57.5
17	65	250	15	8	10	0.52	119, 58	55.8
18	65	250	15	8	20	0.52	128, 79	63.5
19	65	250	15	8	30	0.52	156, 106	66.3
20	65	250	15	8	40	0.52	205, 106	73.8

drug in the solvent, which caused by the increased vapor pressure of the solute (Rehman et al., 2001). As a result, a higher diffusivity and mass transfer were achieved. Consequently, particle size decreases with increasing temperature. On the other hand, the microparticle yield increased as the temperature was heightened from 45 °C to 65 °C. Yield of GA microparticles increased with increase in temperature may be due to the following reason: MPS decreased as the temperature was increased from 35 to 65 °C. Meanwhile, the "soft agglomeration" of nanoparticles is more likely to occur, thus the GA microparticles yield increased. However, nanoparticles agglomerations are easily dispersed by ultrasonic treatment before performing DLS analysis because agglomeration forces are very weak, which can result in a smaller measured value of MPS. Therefore, all following experiments were carried out at the temperature of 65 °C.

The experiment was carried out at various pressures (150, 200, 250, and 300 bar), fixing the temperature at 65 °C, CO_2 flow rate at 10 mL min^{-1} and the concentration of the drug solution at 20 mg mL^{-1}. The influence of CO_2 pressure was shown in Fig. 3b. In case of CO_2 pressure less than 250 bar, a higher pressure results in smaller particles whereas in case of higher pressure (>250 bar) the reverse tendency was found. There was an apparent tendency for MPS to decrease ranging from 283 to 139 nm as pressure increases from 150 to 250 bar. Moreover, the PSD also sharpens as the pressure increases. The same effect was observed also during the SAS of other organic compound (Reverchon and De Marco, 2006). This phenomenon may be due to intensification of diffusion driving force of the SC-CO_2 into the droplets at higher precipitation pressure, which resulted in a higher degree of supersaturation (Kröber and Teipel, 2002), and consequently obtaining precipitation of particles with smaller MPS and narrower particle size distribution. However, when the pressure was increased to an even higher value of 300 bar (as shown in Fig. 3b), the product have larger MPS (209 nm) than those obtained at 250 bar. We speculate that this may because spraying of GA/ethanol cannot be carried out smoothly at huge CO_2 pressure, which resulted in difficulty in forming very small fog droplets of drug solution, consequently, the particles may be particularly prone to aggregation during recrystallization. On the other hand, the results of data analysis demonstrated that the smaller yield of GA was obtained when a higher pressures was used for the precipitation process. This may be because of the initial crystal size was smaller with an increase in pressure, caused by

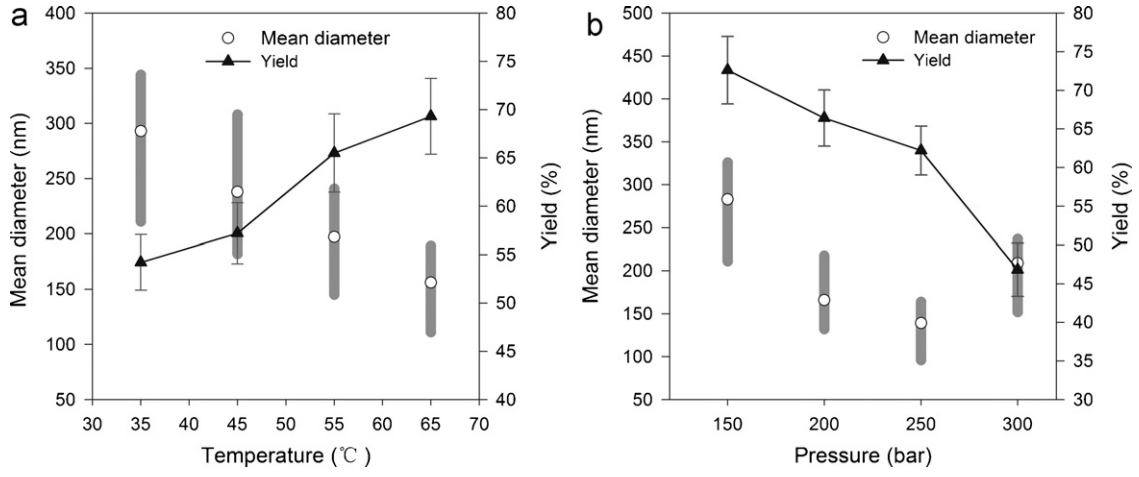

Fig. 3. Influence of pressure (a) and temperature (b) on the mean particle size and total yield (mean ± SD, $n = 3$).

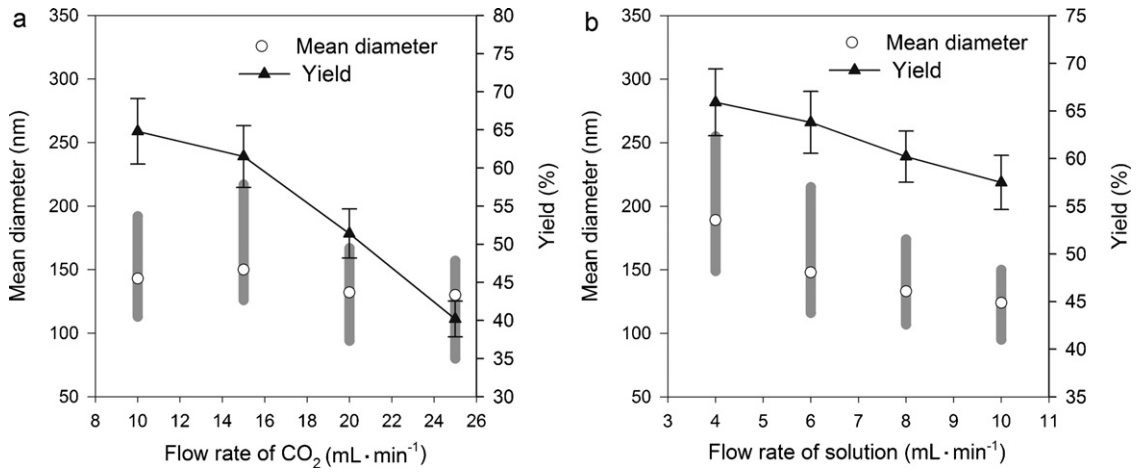

Fig. 4. Influence of flow rate of CO_2 (a) and flow rate of solution (b) on the mean particle size and total yield (mean ± SD, $n = 3$).

increasing GA supersaturation. Meanwhile, greater pressure also makes it easier for the nascent and tiny crystal particles to escape from precipitation chamber.

3.1.2. Effect of flow rates of CO_2 and drug solution

Experiments with different carbon dioxide and drug solution flow rates were performed at the same pressure, temperature, feed concentration. Fig. 4a presents experimental results that demonstrate the effect of CO_2 flow rate on MPS and total yield. The CO_2 flow varied from 10 to 25 mL min^{-1}. MPS of GA microparticles prepared at CO_2 flow 20 and 25 mL min^{-1} (132 and 130 nm) were slightly smaller than those prepared at 10 and 15 mL min^{-1} (143 and 150 nm). This behavior was probably due to the increase in the Reynolds number generated by the CO_2 flow rate, thus turbulence was enhanced (Ghaderi et al., 1999), which resulted in a better mixing between the solvents turbulence, and thus contribute to the precipitation process. However, we did not observe a significant correlation between MPS and CO_2 flow rates. CO_2 flows have an effect but did not seem to play a huge role compared to temperature or pressure. According to Fig. 4a, the total yield at a CO_2 flow rate of 25 mL min^{-1} was lower than that at other CO_2 flow rates, because the precipitates were easily entrained by CO_2 at the higher flow rate. In the following experiment, we will choose 15 mL min^{-1} of CO_2 because turbulence and atomization of liquid are stronger than those prepared at 10 mL min^{-1} of CO_2, which can contribute to the generation of smaller particles. Furthermore, the differences in yield and MPS between 10 mL min^{-1} and 15 mL min^{-1} of CO_2 flow are not great.

The influence of flow rate of drug solution on MPS and total yield was determined by varying the flow rate of solution between 4 and 10 mL min^{-1}. The pressure and temperature condition was fixed at 250 bar and 65 °C. The flow rate of CO_2 was 15 mL min^{-1}. As shown in Fig. 4b, obviously, a higher ethanol solution flow rate leads to a decrease in mean particle size. When solution flow rate increased from 4 to 10 mL min^{-1}, the MPS has changed from 189 to 124 nm. We suppose that these phenomena can be explained by the following reasons. In the first place, a higher flow rate results in a larger capillary number (Eq. (1)) which means the ratio of viscous forces versus surface tension acting across an interface between organic solvent and supercritical CO_2, thus leading to the breakup into smaller droplets (Kröber and Teipel, 2002).

In the second place, the increase in the drug solution flow rate could lead to a better mixing between the drug solution and the supercritical carbon dioxide, thus creating a stronger turbulence. This results in higher supersaturation and consequently a smaller particle diameter.

$$Ca = \frac{\rho \mu^2 d_N}{\sigma Re} \quad (1)$$

where ρ is the solvent density, μ is the velocity, d_N is the nozzle diameter, σ is the surface tension and Re is Reynolds number.

PSD is more dependent on the fluid dynamics features and it results from a balance between micromixing and nucleation/growth kinetics (Lengsfeld et al., 2000). The results (Fig. 4b) shows that narrower PSD was obtained as the solution flow rate increases.

As regards the total yield of GA microparticles, a gradual decreasing tendency was observed toward total yield with increasing flow rate of drug solution. The yield for lower level of flow rate of drug solution was higher.

3.1.3. Effect of concentration of drug solution

The concentration of the drug solution is the parameter that mainly controls the diameter and the polydispersity of GA microparticles. We prepared GA microparticles at various drug concentrations in the range from 10 to 40 mg mL^{-1} (65 °C, 250 bar, F_{CO2} = 15 mL min^{-1} and F_{drug} = 8 mL min^{-1}) to investigate the effect of the drug concentration on the MPS and yield of SAS processed GA (Fig. 5). In terms of the MPS, it was observed that an increase of the concentration of the drug solution caused an increase of the MPS and an enlargement of the PSD. The same tendency was also

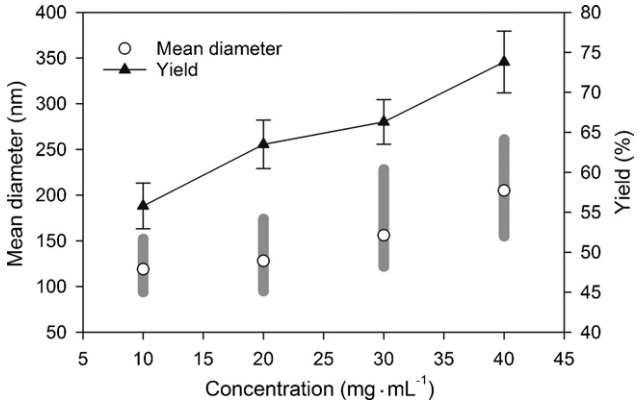

Fig. 5. Influence of drug concentration on the mean particle size and total yield (mean ± SD, $n = 3$).

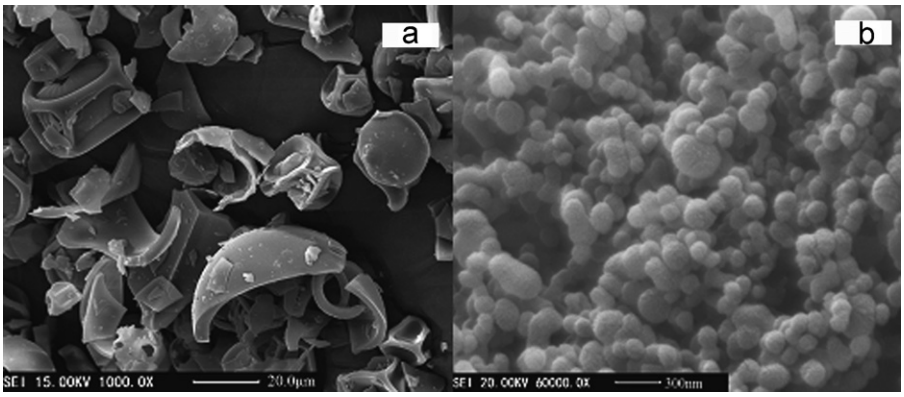

Fig. 6. Scanning electron micrographs of (a) GA raw material and (b) GA microparticles.

reported in the SAS process of other compound (Reverchon and De Marco, 2004). Increasing drug concentrations gives rise to increase of MPS could be related to nucleation and growth processes. Drug concentration affects the size of particles in opposing ways: high drug concentration leads to high supersaturation, which results in a faster nucleation rate and then smaller particles; whereas, high supersaturation also speeds up agglomeration promoting production of bigger particles. As can be seen, agglomeration prevails over nucleation when ranging from 10 to 40 mg mL^{-1}. Higher concentrations lead to the higher particle growth rate and coagulation among the particles. That is to say, particles precipitated by SAS are tight aggregates of nanoparticles instead of the result of a single growth process (Reverchon et al., 2002). With the obtained results, it is possible to conclude that lower GA concentrations can effectively reduce the particle size and narrow the size distribution. In addition, increasing the drug concentration from 10 to 40 mg mL^{-1} resulted in the yield increase of GA microparticles from 55.8% to 73.8%, which indicates drug microparticle of larger size is easier to collect than microparticle of smaller size.

3.2. Morphology

Fig. 6(a) and (b) shows SEM morphology of GA microparticles made using supercritical antisolvent precipitation (65 °C, 250 bar, C_{drug} = 20 mg mL^{-1}, F_{CO2} = 15 mL min^{-1} and F_{drug} = 8 mL min^{-1}) and GA raw material, respectively. MPS and PSD of microparticle has been previously determined using particle size analyzer laser (PSD ranged from 95 and 174 nm, MPS was 128 nm). We can easily observe that most of the microparticles appeared spheres or subglobose with a diameter of about 90–180 nm, nonetheless GA raw materials exhibit an irregular shape, micron-grade particle size and a wide size distribution. Generally speaking, habit and morphology of natural drug powders have a great impact on the bioavailability when they were digested in human metabolism system. Reduced particle size increases the surface Gibbs free energy, conducing to enhance the dissolution rate and dispersion of drug particle. Consequently, SAS recrystallization is capable to produce regular and nanosized GA particles, which might be able to enhance the oral absorption of drug powder.

3.3. X-ray diffraction studies

We investigated crystal structure difference between GA microparticles and raw materials using XRD analyses. As shown in Fig. 7, at the diffraction angles of 2θ = 5–45°, no obvious diffraction peak with very high intensity were observed on the diffraction pattern of GA raw material, but a lot diffraction peak with weak intensity can be observed. This result means that GA raw material has a certain degree of crystallinity, but the degree of crystallinity is weak. Nevertheless, in the case of micronized GA, the weak diffraction peak turn into the weaker peak with very small intensity. This phenomenon indicates that the crystallinity of GA decreased greatly and amorphous state of GA was formed almost entirely by SAS. As far as drug particles are concerned, the amorphous form plays an important role in solubility and the dissolution rate, which usually results in higher solubility and a faster dissolution rate.

3.4. DSC and TG analysis

The DSC is a technique used to measure the temperature and energy variation involved in the phase transitions, which related to the degree of crystallinity and stability of the solid state of drug. TGA is commonly employed to determine characteristics of samples, including degradation temperatures, absorbed moisture content of materials and solvent residues, etc. Simultaneous measurement of DSC and TGA can require interpretations of results which are complementary to each other. The DSC and TGA curves of GA raw materials and GA microparticles were shown in Fig. 8(a) and (b), respectively. According to the DSC curve of raw GA particles, an obvious endotherm peak at 208–240 °C was observed, and we speculate that this peak is attributable to GA decomposition. However, no endotherm was found in the range 100–200 °C, which represented that there do not exist melting and dehydration of GA in the range 100–200 °C. The same behavior has also been reported (Kondo et al., 1984). In order to further confirm conclusion, the TGA result was analyzed. As shown by TGA curve, a gradual weight loss spread out over the entire temperature range. The starting temperature of a sudden weight drop on the TGA curve (the slope of

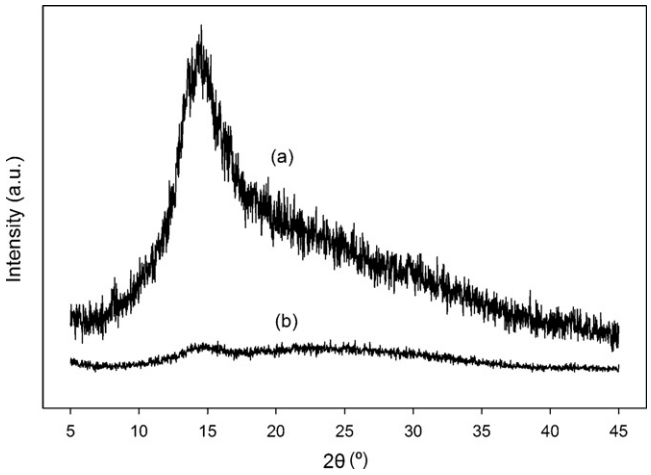

Fig. 7. XRD patterns of (a) GA raw material and (b) GA microparticles.

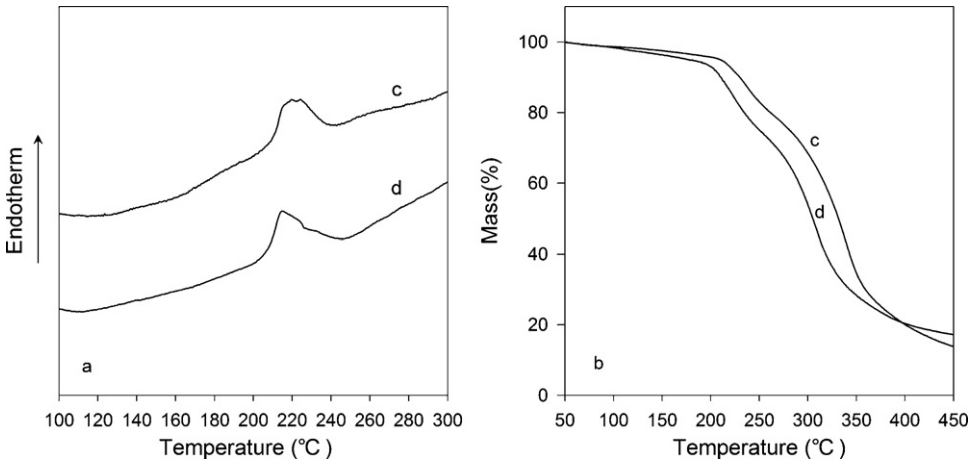

Fig. 8. DSC (a) and TG (b) curve of GA raw material (c) and GA microparticles (d).

the TGA curve increases sharply) was about 208 °C, due to the thermal decomposition of raw GA particles, converting to glycyrrhetinic acid (Sung and Li, 2004). This temperature is in coincidence with DSC signal. However, no obvious weight loss was observed at temperatures below 200 °C, indicating water loss (i.e. dehydration) does not occur. As far as GA microparticles are concerned, there is an endotherm peak at 198–250 °C indicating degradation of GA microparticles. The starting temperature of the endotherm peak was shifted to lower temperature, which had good agreement with TGA results that starting temperature of a sudden weight drop on the TGA curve was lower than GA raw material, the decomposition occurred at about 198 °C. Perhaps this can be explained by the fact that crystallinity convert substantially to amorphous, which is unstable high energy state (Hancock and Zografi, 1997).

3.5. FT-IR spectroscopy

The FT-IR spectra of GA raw material and GA microparticle are compared in Fig. 9. The spectrum showed that absorption peaks of two powders have exactly the same shape and frequency position in the range 400–4000 cm^{-1}, indicating that functional group structure of GA raw material and microparticles have no difference. We can safely draw the conclusion that molecular structure of GA do not change before and after SAS.

3.6. Dissolution studies

The dissolution profiles of the raw GA particles and GA microparticles are shown in Fig. 10. The GA microparticles showed higher dissolution rate than the GA raw particle. The maximum saturation concentration for raw GA particles are approximately 13 mg mL^{-1}, which was reached after 60 min. At the same time, the concentration of GA microparticles just reached saturation point, whereas the maximum saturation concentration of the microparticles was about 71 mg mL^{-1}. The remarkable increase in the dissolution rate can be attributed to amorphous nature. The high internal energy and specific volume of the amorphous state relative to the crystalline state can lead to enhanced dissolution (Hüttenrauch, 1978). In addition, according to the Kelvin equation, as the particle becomes gradually smaller, the surface tension and the molar free energy of particles change, thereby resulting in the increased solubility (Nelson, 1972).

3.7. Bioavailability study

The paired-samples *t* test was used to examine the difference in the oral bioavailability of GA between raw particles and microparticles. All statistical evaluations were performed with SPSS for Windows, version 17.0.0 (SPSS Inc., USA). *P* values less than 0.05 were considered statistically significant in all analyses. Fig. 11 shows the mean plasma concentration–time curve of GA after the oral administration of raw GA particles and GA microparticles to rats at doses of 250 mg kg^{-1}. The plasma concentration profile of

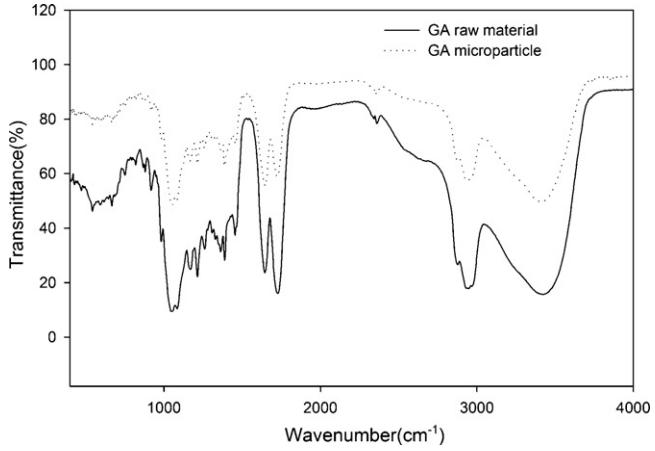

Fig. 9. FT-IR spectra of GA raw material and GA microparticle.

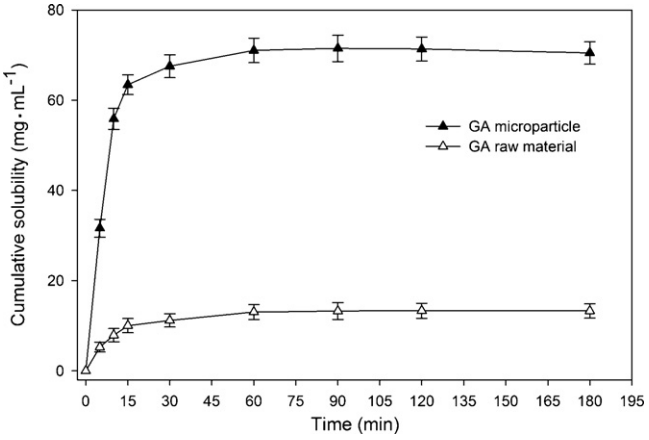

Fig. 10. Dissolution profiles of GA microparticles and compared with original GA.

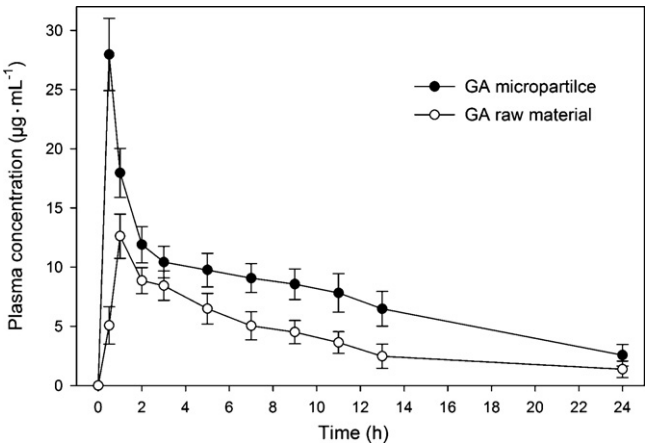

Fig. 11. Mean (±SD) plasma concentration-time curves after oral administration of GA raw material and microparticles suspension at a dose of 80 mg kg^{-1} (n = 6).

Table 2
The mean (±SD) pharmacokinetic parameters of GA when GA microparticles and raw GA particles suspension were orally administered to male rats (n = 6).

	GA raw particles	GA microparticles
t_{max}[a] (h)	1.0 ± 0.12**	0.5 ± 0.05
C_{max}[b] (μg mL^{-1})	12.62 ± 1.87***	27.97 ± 3.06
AUC_{0-t}[c] (μg h mL^{-1})	81.15 ± 11.80***	164.75 ± 25.34
$AUMC_{0-t}$[d] (μg h mL^{-1})	546.44 ± 68.85***	1378.41 ± 179.24
MRT_{0-t}[e] (h)	6.73 ± 0.75*	8.36 ± 0.84

* $p < 0.05$, using compare means followed by paired-samples t-test.
** $p < 0.01$, using compare means followed by paired-samples t-test.
*** $p < 0.001$, using compare means followed by paired-samples t-test.
[a] Time of peak concentration.
[b] Peak of maximum concentration.
[c] Area under the concentration time profile curve until last observation.
[d] Area under moment curve computed to the last observation.
[e] Mean residence time.

GA microparticles represents significantly greater improvement of drug absorption than the raw GA particles, and the plasma concentrations of microparticles at 0.5–24 h were consistently higher than raw particles. The bioavailability parameters are listed in Table 2. The results obtained revealed that, GA microparticles showed the higher C_{max} (27.97 ± 3.06 μg mL^{-1}) at T_{max} of 0.5 h, while raw GA particles showed the lower C_{max} (12.62 ± 1.87 μg mL^{-1}) at T_{max} of 1.0 h. The mean AUC_{0-t} value of GA microparticles was twice the value of raw GA particles.

Statistically, the difference in T_{max} of GA microparticles was highly significant ($p < 0.01$) when compared to T_{max} of raw particles. The difference in C_{max} of GA formulation was extremely significant ($p < 0.001$) when compared with C_{max} of raw particles. It was also observed that AUC_{0-t} and $AUMC_{0-t}$ of GA microparticles were 164.75 ± 25.34 μg h mL^{-1} and 1378.41 ± 179.24 μg h mL^{-1}, respectively, and the difference was extremely significant ($p < 0.001$) as compared with AUC_{0-t} (81.15 ± 11.80 μg h mL^{-1}) and $AUMC_{0-t}$ (546.44 ± 68.85 μg h mL^{-1}) of raw particles. The difference in the values of MRT_{0-t} is significantly different ($p < 0.05$) when compared with MRT_{0-t} of raw particles. The reason for this clear difference of bioavailability parameters is considered to be as follows: (a) microparticles have higher specific surface area of than raw particles; (b) the drug in a molecular/amorphous state increase the dissolution rate; (c) more particle size reduction of microparticles, which improves uptake and bioavailability of drug.

4. Conclusions

Solid dispersion microparticles of poorly water-soluble GA were prepared by using the SAS methods. We found that operating parameters (such as temperature, pressure and liquid concentration, etc.) have influences on MPS and yield of GA microparticles. According to results of *in vitro* dissolution test and *in vivo* bioavailability study in rats, we can confirm GA microparticles have higher solubility and better bioavailability than GA raw materials. The SAS process would be a feasible and efficient pathway in enhancing the solubility of poorly water-soluble GA with high dissolution rate. However, previous studies have found that excessive intake of licorice can cause hypokalemia and hypertension and generally, the onset and severity of symptoms depend on the dose and duration of licorice intake (Mumoli and Cei, 2008). Therefore, concerning the distinct increase in AUC and mean residence time of GA when microparticles are administered, we suggest that the regular dose of GA (in case of human use) in form of produced microparticles should be diminished to avoid the increase of incidence of licorice-induced hypokalemia and hypertension (in case of chronic therapy).

Acknowledgements

The authors thank anonymous reviewers for their insightful comments and careful corrections. The authors also thank the National Key Technology R&D Program (2006BAD18B04) and the China-Germany Inter-Governmental Cooperation Program (CHN3/028) for financial support.

References

Cherng, J.M., Lin, H.J., Hsu, Y.H., Hung, M.S., Lin, J.C., 2004. A quantitative bioassay for HIV-1 gene expression based on UV activation: effect of glycyrrhizic acid. Antiviral Res. 62, 27–36.
Cui, Q.H., Cui, J.H., Zhang, J.J., 2008. Preparation of coated tablets of glycyrrhetic acid-HP-beta-cyclodextrin tablets for colon-specific release. Chin. J. Chin. Mater. Med. 33, 2339–2343.
Finney, R.S.H., Somers, G.F., 1958. The anti-inflammatory activity of glycyrrhetinic acid and derivatives. J. Pharm. Pharmacol. 10, 613–620.
Ghaderi, R., Artursson, P., Carlfors, J., 1999. Preparation of biodegradable microparticles using solution-enhanced dispersion by supercritical fluids (SEDS). Pharm. Res. 16, 676–681.
Hancock, B.C., Zografi, G., 1997. Characteristics and significance of the amorphous state in pharmaceutical systems. J. Pharm. Sci. 86, 1–12.
Hüttenrauch, R., 1978. Molekulargalenik als grundlage moderner arzneiformung. Acta Pharm. Technol. 6, 55–127.
Kondo, M., Minamino, H., Otani, Y., Miyashita, A., Okada, K., Kuramoto, T., 1984. Clear liquid skin cosmetic compositions. Google patents, patent no. 4481187.
Kröber, H., Teipel, U., 2002. Materials processing with supercritical antisolvent precipitation: process parameters and morphology of tartaric acid. J. Supercrit. Fluids 22, 229–235.
Lengsfeld, C., Delplanque, J., Barocas, V., Randolph, T., 2000. Mechanism governing microparticle morphology during precipitation by a compressed antisolvent: atomization vs nucleation and growth. J. Phys. Chem. B 104, 2725–2735.
Li, M., Rouaud, O., Poncelet, D., 2008. Microencapsulation by solvent evaporation: state of the art for process engineering approaches. Int. J. Pharm. 363, 26–39.
Lin, A.H., Liu, Y.M., Huang, Y., Sun, J.B., Wu, Z.F., Zhang, X.F., Ping, Q.N., 2008. Glycyrrhizin surface-modified chitosan nanoparticles for hepatocyte-targeted delivery. Int. J. Pharm. 359, 247–253.
Lin, G., Nnane, I.P., Cheng, T.Y., 1999. The effects of pretreatment with glycyrrhizin and glycyrrhetinic acid on the retrorsine-induced hepatotoxicity in rats. Toxicon 37, 1259–1270.
Ma, P., Fu, Z., Su, Y., Zhang, J., Wang, W., Wang, H., Wang, Y., Zhang, Q., 2009. Modification of physicochemical and medicinal characterization of Liuwei Dihuang particles by ultrafine grinding. Powder Technol. 191, 194–199.
Mumoli, N., Cei, M., 2008. Licorice-induced hypokalemia. Int. J. Cardiol. 124, e42–e44.
Nelson, K.G., 1972. The Kelvin equation and solubility of small particles. J. Pharm. Sci. 61, 479–480.
Nishino, H., Kitagawa, K., Iwashima, A., 1984. Antitumor-promoting activity of glycyrrhetic acid in mouse skin tumor formation induced by 7, 12-dimethylbenz [a] anthracene plus teleocidin. Carcinogenesis 5, 1529.
Rehman, M., Shekunov, B.Y., York, P., Colthorpe, P., 2001. Solubility and precipitation of nicotinic acid in supercritical carbon dioxide. J. Pharm. Sci. 90, 1570–1582.
Reverchon, E., De Marco, I., 2004. Supercritical antisolvent micronization of Cefonicid: thermodynamic interpretation of results. J. Supercrit. Fluids 31, 207–215.
Reverchon, E., De Marco, I., 2006. Supercritical antisolvent precipitation of cephalosporins. Powder Technol. 164, 139–146.
Reverchon, E., De Marco, I., Della Porta, G., 2002. Rifampicin microparticles production by supercritical antisolvent precipitation. Int. J. Pharm. 243, 83–91.

Rizi, K., Green, R.J., Donaldson, M., Williams, A.C., 2010. Production of pH-responsive microparticles by spray drying: investigation of experimental parameter effects on morphological and release properties. J. Pharm. Sci. 100, 566–579.
Shibata, S., 2000. A drug over the millennia: pharmacognosy, chemistry, and pharmacology of licorice. Yakugaku Zasshi 120, 849–862.
Sung, M.W., Li, P.C.H., 2004. Chemical analysis of raw, dry-roasted, and honey-roasted licorice by capillary electrophoresis. Electrophoresis 25, 3434–3440.
Werling, J.O., Debenedetti, P.G., 1999. Numerical modeling of mass transfer in the supercritical antisolvent process. J. Supercrit. Fluids 16, 167–181.
Yang, L., Huang, J., Zu, Y., Ma, C., Wang, H., Sun, X., Sun, Z., 2011. Preparation and radical scavenging activities of polymeric procyanidins nanoparticles by a supercritical antisolvent (SAS) process. Food Chem. 128, 1152–1159.
Yuan, Q.Y., Liu, H.Y., Zhou, K., Shi, B.J., 2005. Pharmacokinetics of glycyrrhizin liposome and glycyrrhizin. Zhongguo Xinyao Zazhi 7, 903–905.
Zhao, C., Wang, L., Zu, Y., Li, C., Liu, S., Yang, L., Zhao, X., Zu, B., 2011. Micronization of Ginkgo biloba extract using supercritical antisolvent process. Powder Technol. 209, 73–80.